
Article:
Vignollet, J, May, S and de Borst, R orcid.org/0000-0002-3457-3574 (2015) On the numerical integration of isogeometric interface elements. International Journal for Numerical Methods in Engineering, 102 (11). pp. 1733-1749. ISSN 0029-5981

https://doi.org/10.1002/nme.4867

INTERNATIONAL JOURNAL FOR NUMERICAL METHODS IN ENGINEERING
Int. J. Numer. Meth. Engng 2014; **00**:1–17
Published online in Wiley InterScience (www.interscience.wiley.com). DOI: 10.1002/nme

On the numerical integration of isogeometric interface elements

Julien Vignollet, Stefan May and René de Borst*†

School of Engineering, University of Glasgow, Glasgow G12 8LT, UK

SUMMARY

Zero-thickness interface elements are commonly used in computational mechanics to model material interfaces or to introduce discontinuities. The latter class requires the existence of a non-compliant interface prior to the onset of fracture initiation. This is accomplished by assigned a high dummy stiffness to the interface prior to cracking. This dummy stiffness is known to introduce oscillations in the traction profile when using Gauss quadrature for the interface elements, but these oscillations are removed when resorting to a Newton-Cotes integration scheme [1]. The traction oscillations are aggravated for interface elements that use B-splines or NURBS as basis functions (isogeometric interface elements), and worse, do not disappear when using Newton-Cotes quadrature. An analysis is presented of this phenomenon, including eigenvalue analysis, and it appears that the use of lumped integration (at the control points) is the only way to avoid the oscillations in isogeometric interface elements. New findings have also been obtained for standard interface elements, for example that oscillations occur in the relative displacements at the interface irrespective of the value of the dummy stiffness. Copyright © 2014 John Wiley & Sons, Ltd.

Received . . .

KEY WORDS: Interface elements; isogeometric analysis; traction oscillations

1. INTRODUCTION

Zero-thickness interface elements are ubiquitous in finite element analysis. They have been used frequently to characterise material interfaces and to introduce discontinuities in bodies, e.g. cracks, shear bands, or faults since the early 1970s [2]. Interface elements have proven to be useful in the analysis of concrete fracture [3], of delamination in composite materials and debonding of adhesive layers [4, 5, 6, 7], and for analysing dynamic rupture using plastic slip models [8]. They are currently available in most commercial finite element packages. In combination with their ease of use and general robustness this has made interface elements popular for a wide range of applications.

Interface elements are well suited to describe stationary discontinuities, or situations where the evolution of the discontinuity is known a priori, for example because the crack path is known from experimental evidence [3], or because the evolution of the discontinuity is known from the location of material interfaces, as in lamellar structures. An important step towards describing arbitrary crack propagation was made in [9], where interface elements were inserted between all continuum elements. Although powerful, it is an expensive solution, and moreover, it can add too much compliance to the structure. Indeed, when interface elements are used to describe fracture, they must be equipped with a high stiffness prior to the onset of cracking in order to minimise unphysical deformations in the interface. This is avoided when interface elements are generated during crack propagation as in [10], but this can require elaborate remeshing procedures at each

†E-mail: Rene.DeBorst@glasgow.ac.uk
*Correspondence to: René de Borst, School of Engineering, University of Glasgow, Glasgow G12 8LT, UK

loading step. Another way to introduce interfaces is to exploit the discontinuous Galerkin approach, as was done in [11, 12], see also [13].

Exploiting the possibility to lower the order of spline functions Verhoosel *et al.* [14] have introduced discontinuities in isogeometric analysis [15]. This idea was further elaborated in [16], where an interface element was developed that is suitable for the analysis of mechanical and poromechanical fracture problems, and in [17, 18] in the context of delamination. Unlike the original paper, the formulation in [16] exploits Bézier extraction, which makes it easy to implement in standard finite element software, as it is then cast in a format that is compatible with standard finite element datastructures [19, 20].

It was noticed in [16] that prior to crack initiation, oscillations appeared in the traction profiles in the interface elements. In principle, this is nothing new, and it has been known for long that such oscillations emerge when using a high value of the dummy stiffness in combination with a Gauss numerical integration scheme for the interface [1]. The observation that the remedy commonly applied in standard finite element analysis, namely to replace Gauss quadrature by Newton-Cotes integration, did not remove the traction oscillations, is, however, disturbing.

Herein, we carry out an in-depth investigation of the appearance of oscillations in the traction profiles of non-compliant, isogeometric interface elements. In passing, we revisit some conclusions regarding traction oscillations in standard interface elements [1]. To provide a proper setting, we start with a concise summary of standard interface elements in Section 2, and recall evidence on oscillations in traction profiles from the literature. Next, in Section 3, we succinctly review some basic concepts of isogeometric analysis, including the concept of Bézier extraction. Section 4 constitutes the core of the paper and presents two-dimensional and three-dimensional analyses of isogeometric interface elements, confirming that isogeometric interface elements inherit the traction oscillations from standard interface elements, and, in fact, aggravate the situation. To further investigate the issue, analyses have also been carried out for elements that are equipped with splines as basis functions, but have conventional $\mathcal{C}^0$-continuity at element boundaries, and for isogeometric interface elements where the centre control point has been shifted. The computations are augmented by eigenvalue analyses. The use of lumped integration turns out to be a rigorous solution for isogeometric interface elements, as will be demonstrated in two and in three dimensions. Furthermore, an investigation will be carried out to oscillations that occur in the relative displacements at the interface, an issue that has not been paid attention to so far.

2. REVISITING INTERFACE ELEMENTS

2.1. Formulation

We consider a body Ω shown in Figure 1, with Dirichlet boundary conditions at Γ_u and Neumann boundary conditions at Γ_t. An interface Γ_d divides the domain into two parts, Ω^+ and Ω^-, respectively, such that $\Omega = \Omega^+ \cup \Omega^-$, and is equipped with a local coordinate system $(\mathbf{n}, \mathbf{s}, \mathbf{t})$, where $\mathbf{n}$ is normal vector to the interface, and $\mathbf{s}$ and $\mathbf{t}$ define the directions tangential to the interface. For future reference we make distinction between Γ_d^+, the side of Γ_d that borders Ω^+, and Γ_d^-, the side of Γ_d that borders Ω^-.

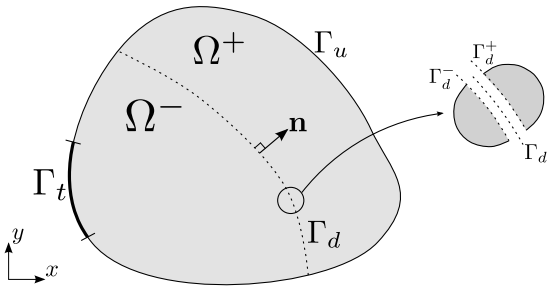

Figure 1. Schematic representation of a body Ω crossed by a discontinuity Γ_d

DOI: 10.1002/nme

Without loss of generality we can restrict the present treatment to static loading conditions, so that the balance of linear momentum reads:

$$\nabla \cdot \boldsymbol{\sigma}(\mathbf{x}) = \mathbf{0} \qquad \mathbf{x} \in \Omega, \tag{1}$$

where $\boldsymbol{\sigma}$ denotes the Cauchy stress at a material point $\mathbf{x} \in \Omega$. The problem is closed by imposing boundary conditions at the external boundaries Γ_u and Γ_t, and on the discontinuity Γ_d:

$$\mathbf{u}(\mathbf{x}) = \bar{\mathbf{u}} \qquad \mathbf{x} \in \Gamma_u, \tag{2a}$$
$$\mathbf{n}(\mathbf{x}) \cdot \boldsymbol{\sigma}(\mathbf{x}) = \bar{\mathbf{t}}(\mathbf{x}) \qquad \mathbf{x} \in \Gamma_t, \tag{2b}$$
$$\mathbf{n}(\mathbf{x}) \cdot \boldsymbol{\sigma}(\mathbf{x}) = \mathbf{t}_d^l(\llbracket \mathbf{u} \rrbracket(\mathbf{x})) \qquad \mathbf{x} \in \Gamma_d. \tag{2c}$$

According to Equation (2c), the traction $\mathbf{t}_d^l$, defined in the local coordinate system of the interface Γ_d is a function of the displacement jump $\llbracket \mathbf{u} \rrbracket$ at the interface. The latter can be decomposed in the normal jump $\llbracket u_n \rrbracket$, and the slidings $\llbracket u_s \rrbracket$ and $\llbracket u_t \rrbracket$, respectively:

$$\llbracket \mathbf{u} \rrbracket = \llbracket u_n \rrbracket \mathbf{n} + \llbracket u_s \rrbracket \mathbf{s} + \llbracket u_t \rrbracket \mathbf{t}, \tag{3}$$

where, for clarity of the notation, the explicit dependence of quantities on the spatial coordinate $\mathbf{x}$ has been omitted, and the convention $\llbracket \bullet \rrbracket = (\bullet)^+ - (\bullet)^-$ was adopted to denote a jump in a field quantity, $(\bullet)^+$ and $(\bullet)^-$ being evaluated at Γ_d^+ and Γ_d^-, respectively. Employing the rotation matrix $\mathbf{R} = \left[\mathbf{n}^{\mathrm{T}}, \mathbf{s}^{\mathrm{T}}, \mathbf{t}^{\mathrm{T}}\right]$, the interface traction $\mathbf{t}_d$ referred to the global coordinate system can be derived as:

$$\mathbf{t}_d(\llbracket \mathbf{u} \rrbracket) = \mathbf{R}^{\mathrm{T}} \mathbf{t}_d^l(\llbracket \mathbf{u} \rrbracket). \tag{4}$$

The interface traction $\mathbf{t}_d^l$ is generally a (strongly) nonlinear function of the displacement jump $\llbracket \mathbf{u} \rrbracket$,

$$\mathbf{t}_d^l(\llbracket \mathbf{u} \rrbracket) = \mathbf{t}_d^l. \tag{5}$$

When considering material interfaces there is usually a physically non-zero compliance from the onset of deformation and the undeformed state is characterised by: $\mathbf{t}_d^l(\mathbf{0}) = \mathbf{0}$.

When interface elements are used to model cracks that nucleate in a hitherto intact medium, the interface compliance is zero till the onset of cracking. A zero interface compliance corresponds to an infinite interface stiffness and this is usually approximated by assigning high values to the 'dummy' stiffnesses k_n, k_s and k_t in the normal and the sliding directions. It is noted that the values of the dummy stiffnesses are problem and length-scale dependent, but must be chosen as high as possible. Prior to the onset of cracking the interface stiffness matrix $\mathbf{D}_i$ in the local coordinate system then attains the format:

$$\mathbf{D}_i = \begin{bmatrix} k_n & 0 & 0 \\ 0 & k_s & 0 \\ 0 & 0 & k_t \end{bmatrix} \tag{6}$$

and

$$\mathbf{t}_d^l = \mathbf{D}_i \llbracket \mathbf{u} \rrbracket. \tag{7}$$

Inserting Equation (7) into Equation (4) results in:

$$\mathbf{t}_d(\llbracket \mathbf{u} \rrbracket) = \mathbf{R}^{\mathrm{T}} \mathbf{D}_i \llbracket \mathbf{u} \rrbracket. \tag{8}$$

The weak formulation is obtained in a standard fashion by multiplying Equation (1) by a virtual displacement field $\delta\mathbf{u}$. Application of the divergence theorem and exploiting the external boundary conditions (2(a))–(2(b)) then leads to:

$$\int_{\Gamma_t} \bar{\mathbf{t}} \cdot \delta\mathbf{u} \mathrm{d}\Gamma_t + \int_{\Gamma_d^+} \mathbf{t}_d \cdot \delta\mathbf{u} \mathrm{d}\Gamma_d^+ + \int_{\Gamma_d^-} \mathbf{t}_d \cdot \delta\mathbf{u} \mathrm{d}\Gamma_d^- - \int_{\Omega} \boldsymbol{\sigma} : \nabla(\delta\mathbf{u}) \mathrm{d}\Omega = 0. \tag{9}$$

DOI: 10.1002/nme

Since we have traction continuity, i.e. the same interface traction $\mathbf{t}_d$ acts on Γ_d^- and on Γ_d^+, we can rewrite Equation (9) as:

$$\int_\Omega \boldsymbol{\sigma} : \delta\boldsymbol{\varepsilon} \mathrm{d}\Omega + \int_{\Gamma_d^+} \mathbf{t}_d \cdot [\![\delta\mathbf{u}]\!] \mathrm{d}\Gamma_d = \int_{\Gamma_t} \bar{\mathbf{t}} \cdot \delta\mathbf{u} \mathrm{d}\Gamma_t, \tag{10}$$

with $[\![\delta\mathbf{u}]\!]$ the virtual displacement jump, and $\delta\boldsymbol{\varepsilon}$ the virtual strain tensor, which is derived adopting the usual assumption of small displacement gradients.

We subsequently discretise the domain into E_b elements for the bulk and E_d interface elements,

$$\Omega = \bigcup_{e=1}^{E_b} \Omega^e, \qquad \Gamma_d = \bigcup_{e=1}^{E_d} \Gamma_d^e, \tag{11}$$

and interpolate the displacement within each element as follows:

$$\mathbf{u} = \mathbf{N}\mathbf{u}^e, \tag{12}$$

with $\mathbf{u}^e$ a vector that contains the element nodal displacements and $\mathbf{N}$ the matrix that contains the corresponding shape functions, which can either derive from a standard Lagrange interpolation, or from an isogeometric approach, utilising B-splines for example. Exploiting the usual formalism the $\mathbf{B}$-matrix can be derived which contains the derivatives of the shape functions, and the relation between the strains $\boldsymbol{\varepsilon}$ and the nodal displacements $\mathbf{u}^e$ reads:

$$\boldsymbol{\varepsilon} = \mathbf{B}\mathbf{u}^e. \tag{13}$$

Next, the operator $\mathbf{M}$ is constructed, which evaluates the jump at the interface. It operates on the nodal displacements $\mathbf{u}_i^e$ at each side of the interface:

$$[\![\mathbf{u}]\!] = \mathbf{M}\mathbf{u}_i^e. \tag{14}$$

As an example we take the one-dimensional quadratic interface element of Figure 2. The array that contains the displacements of the interface element takes the form $\mathbf{u}_i^e = \big\{\{\mathrm{NS}_1\}, \{\mathrm{NS}_2\}, \{\mathrm{NS}_3\}\big\}$, where for each of the three node-sets $\{\mathrm{NS}_i\} = \{u_i^-, u_i^+, v_i^-, v_i^+\}$, so that:

$$\mathbf{M} = \begin{bmatrix} -N_1 & N_1 & 0 & 0 & -N_2 & N_2 & 0 & 0 & -N_3 & N_3 & 0 & 0 \\ 0 & 0 & -N_1 & N_1 & 0 & 0 & -N_2 & N_2 & 0 & 0 & -N_3 & N_3 \end{bmatrix}. \tag{15}$$

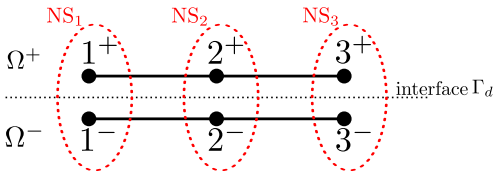

Figure 2. A quadratic one-dimensional interface element. The lines $\{1^+, 2^+, 3^+\}$ and $\{1^-, 2^-, 3^-\}$ coincide, but are shifted for visualisation purposes.

We finally introduce the discretisation of Equation (11), Equation (8), and the operators defined in Equations (12)–(15). The internal force vector can then be evaluated as follows:

$$\mathbf{f}^{\text{int}} = \sum_{e=1}^{E_b} \int_{\Omega^e} \mathbf{B}^{\mathrm{T}} \boldsymbol{\sigma} \mathrm{d}\Omega + \sum_{e=1}^{Ed} \int_{\Gamma_d^e} \mathbf{M}^{\mathrm{T}} \mathbf{R}^{\mathrm{T}} \mathbf{t}_d([\![\mathbf{u}]\!]) \mathrm{d}\Gamma_d \tag{16a}$$

$$= \sum_{e=1}^{E_b} \int_{\Omega^e} \mathbf{B}^{\mathrm{T}} \mathbf{D}_b \mathbf{B}\mathbf{u}^e \mathrm{d}\Omega + \sum_{e=1}^{Ed} \int_{\Gamma_d^e} \mathbf{M}^{\mathrm{T}} \mathbf{R}^{\mathrm{T}} \mathbf{D}_i \mathbf{M}\mathbf{u}_i^e \mathrm{d}\Gamma_d, \tag{16b}$$

DOI: 10.1002/nme

where $\mathbf{D}_b$ is the material stiffness matrix of the bulk material. The stiffness matrix is obtained in a standard manner, i.e. by linearisation of the internal force vector:

$$\mathbf{K} = \frac{\partial \mathbf{f}^{\text{int}}}{\partial \mathbf{u}} = \sum_{e=1}^{E_b} \int_{\Omega^e} \mathbf{B}^{\mathrm{T}} \mathbf{D}_b \mathbf{B} \mathrm{d}\Omega + \sum_{e=1}^{E_i} \int_{\Gamma_d^e} \mathbf{M}^{\mathrm{T}} \mathbf{R}^{\mathrm{T}} \mathbf{D}_i \mathbf{R} \mathbf{M} \mathrm{d}\Gamma_d. \tag{17}$$

2.2. Spurious traction oscillations at the interface

As discussed in the preceding, traction profiles along interfaces will exhibit spurious oscillations for high values of the dummy stiffness. As analysed in detail in Reference [1] this occurs in particular when Gauss integration is used for evaluating the integrals that arise when formulating the interface elements. A classical example is the notched beam subjected to three-point bending shown in Figure 3a [1, 16]. The simply supported beam is divided by an interface along its centreline, and is loaded by a concentrated load at the centre. The beam is 100 mm thick, and the material is characterised by a Young's modulus E = 2 GPa and a Poisson's ratio ν = 0.2. The traction profiles are shown in Figure 3b for values of the dummy stiffness in the normal direction that vary from $k_n = 10^3$ N/mm^2 to $k_n = 10^5$ N/mm^2. Spurious oscillations occur in the traction profile near the tip of the notch for $k_n > 10^3$ N/mm^2. When the dummy stiffness is further increased the oscillations become more pronounced and tend to propagate upwards.

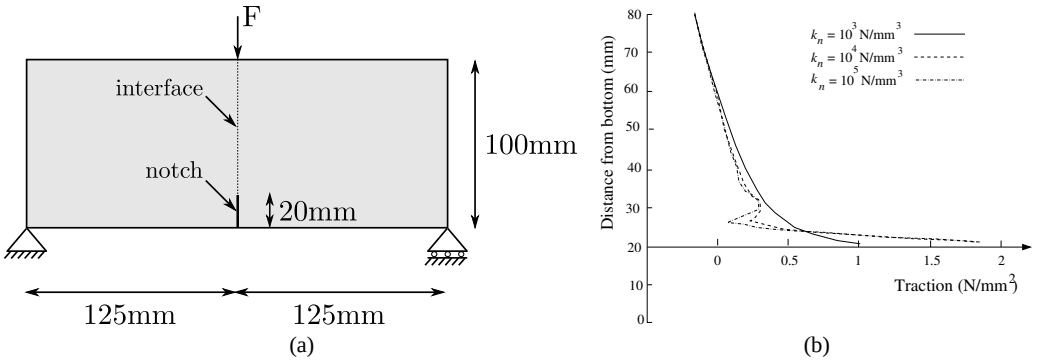

Figure 3. (a) Geometry and boundary conditions for the notched beam subject to three-point bending. (b) Traction profiles along the interface for different values of the dummy stiffness k_n using standard linear four-noded elements and Gauss integration.

It has been shown in [1] for two-dimensional and three-dimensional configurations (hence for one-dimensional and two-dimensional interfaces) that these traction oscillations disappear when using a Newton-Cotes integration scheme instead of the traditional Gauss quadrature. A possible explanation was suggested by inspecting the structure of the stiffness matrix of the interface element, the second term in Equation (17). For instance, for a Gauss integration scheme, the part of the stiffness matrix of a quadratic one-dimensional interface elements of length l that relates to the normal displacements u^+ and u^- takes the following form (in the local coordinate system):

$$\mathbf{K}^{\text{FEM}}_{\text{Gauss}} = \frac{l}{15} \begin{bmatrix} 4k_n & -4k_n & 2k_n & -2k_n & -k_n & k_n \\ -4k_n & 4k_n & -2k_n & 2k_n & k_n & -k_n \\ 2k_n & -2k_n & 16k_n & -16k_n & 2k_n & -2k_n \\ -2k_n & 2k_n & -16k_n & 16k_n & -2k_n & 2k_n \\ -k_n & k_n & 2k_n & -2k_n & 4k_n & -4k_n \\ k_n & -k_n & -2k_n & 2k_n & -4k_n & 4k_n \end{bmatrix}. \tag{18}$$

DOI: 10.1002/nme

On the other hand, for a Newton-Cotes scheme, we obtain:

$$\mathbf{K}^{\text{FEM}}_{\text{Newton-Cotes}} = \frac{l}{3}\begin{bmatrix} k_n & -k_n & 0 & 0 & 0 & 0 \\ -k_n & k_n & 0 & 0 & 0 & 0 \\ 0 & 0 & 4k_n & -4k_n & 0 & 0 \\ 0 & 0 & -4k_n & 4k_n & 0 & 0 \\ 0 & 0 & 0 & 0 & k_n & -k_n \\ 0 & 0 & 0 & 0 & -k_n & k_n \end{bmatrix}. \tag{19}$$

Direct inspection of Equations (18) and (19) reveals that the Newton-Cotes integration scheme fully decouples the contributions of each node-set. That is, each degree of freedom is coupled to the other five degrees of freedom when using the Gauss integration scheme, while it is only coupled to that on the other side of the discontinuity for the Newton-Cotes scheme. This decoupling is also observed when investigating the eigenmodes of the interface elements. Figure 4b shows that for the Newton-Cotes integration scheme, the eigenmodes exhibit a clear uncoupled structure, where each of the six non-zero eigenmodes consists of an elementary deformation of the individual node-sets, either an opening (modes 1-3) or a sliding (modes 4-6), where it is noted that the eigenvalue analyses have been carried out for the full stiffness matrix, i.e. including the stiffness terms belonging to the v^+ and v^- displacements. The modes resulting from the Gauss integration scheme are shown in Figure 4a. We observe that each of the three normal modes and each of the three shear modes triggers deformations at more than one node-set. In [1] the emergence of traction oscillations for Gauss integration was attributed to this property.

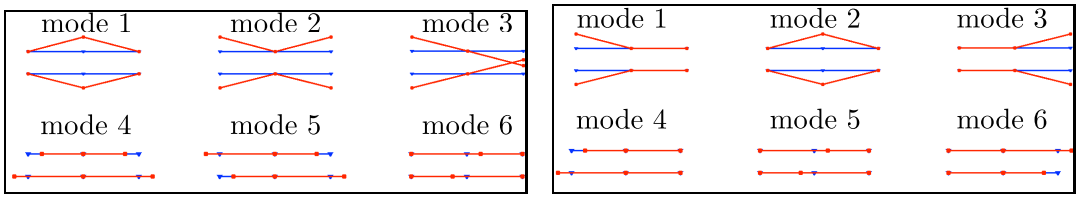

(a) Gauss integration (b) Newton-Cotes integration

Figure 4. Eigenmodes of one-dimensional quadratic interface elements

3. EXTENSION TO $\mathcal{C}^1$-CONTINUOUS INTERFACE ELEMENTS

3.1. Isogeometric interface elements: B-splines and the Bézier operator

We will first give a succinct recapitulation of isogeometric interface elements, see [14, 16] for more details. The idea of isogeometric analysis (IGA) is to use the shape functions used for describing the geometry in Computer Aided Design (CAD) packages, e.g., B-splines, NURBS or T-splines, also as basis functions for the ensuing finite element analysis. In remainder we limit ourselves to B-splines for simplicity, but similar results are anticipated when using NURBS or T-splines.

A univariate B-spline $\mathbf{S}_p$ of order p, parametrised using ξ, is defined as a linear combination of n basis functions:

$$\mathbf{S}_p(\xi) = \sum_{i=1}^{n} N_{i,p}(\xi)\mathbf{P}_i = \mathbf{N}_p(\xi)\mathbf{P}, \tag{20}$$

with $N_{i,p}$ and $\mathbf{P}_i$, $i \in [1, n]$, the n shape functions and control points, respectively, which define the B-spline. $\mathbf{N}_p$ and $\mathbf{P}$ are the matrices that gather the shape functions and the control points. In this study, the location of the control points is evaluated using the Greville's abscissae [21], which ensures a constant Jacobian in each element. The basis functions $N_{i,p}(\xi)$ are evaluated with the Cox-de Boor recursion formula [22, 23]. B-splines are piecewise polynomials parametrised over a knot vector $\Xi = [\xi_1, \xi_2, \cdots, \xi_{n+p+1}]$. Knot values ξ_i are ordered in a non-decreasing manner in a knot vector, and each knot interval of strictly positive length represents an element. Knots can be

DOI: 10.1002/nme

repeated in order to decrease the continuity along a B-spline. B-splines are $p - m_i$ times continuous, where m_i is the multiplicity of knot i. Accordingly, a quadratic ($p = 2$) B-spline is $\mathcal{C}^1$-continuous if the knot vector does not contain repeated knot values ($m_i = 1$). When a knot value is repeated twice, $m_i = 2$, and the B-spline becomes $\mathcal{C}^0$-continuous. Finally, for a multiplicity $m_i = p + 1 = 3$, a discontinuity is introduced between elements. For example, the quadratic B-spline shape functions associated with the knot vector $\Xi = [0, 0, 0, \frac{1}{12}, \frac{2}{12}, \cdots, \frac{1}{2}, \frac{1}{2}, \frac{1}{2}, \cdots, 1, 1, 1]$ contain a discontinuity at $\xi = 0.5$, see Figure 5.

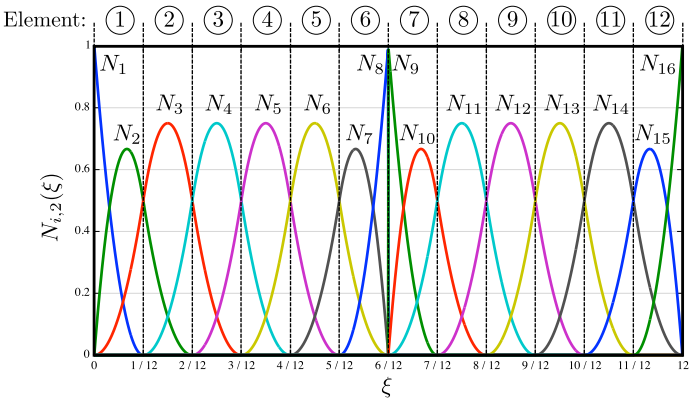

Figure 5. Quadratic shape functions for knot vector $\Xi = [0, 0, 0, \frac{1}{12}, \frac{2}{12}, \cdots, \frac{1}{2}, \frac{1}{2}, \frac{1}{2}, \cdots, 1, 1, 1]$.

Figure 5 shows that, unlike the Lagrange shape functions in standard finite element analysis, B-splines usually extend over more than one element. It is this property which allows for higher continuity across element boundaries, but makes isogeometric analysis not directly amenable to standard finite element datastructures, where shape functions (and many other properties) are stored per element. Use of the Bézier extraction operator [19, 20] solves this issue. The procedure exploits the fact that B-splines, and hence also NURBS and T-splines, can be expressed as a linear combination of Bernstein polynomials of the same order. The Bernstein polynomials span a single element and have the same value within each element, cf. Figure 6a, and therefore need to be evaluated only once. Consequently, if $\mathbf{B}$ contains the set of Bernstein basis functions, the shape function matrix for each element can be expressed using the Bézier extraction operator $\mathbf{C}^e$, which is constant per element, as follows:

$$\mathbf{N}^{\mathbf{e}}_{\mathbf{p}}(\xi) = \mathbf{C}^e\mathbf{B}\Big(\tilde{\xi}(\xi)\Big), \tag{21}$$

where $\tilde{\xi}(\xi)$ denotes the mapping to the parent domain. For example, the non-zero shape functions in element 3 of the B-spline mesh shown in Figure 5 are N_3, N_4 and N_5. The Bézier operator therefore reads:

$$\mathbf{N}^3_2(\xi) = \begin{Bmatrix} N_3(\xi) \\ N_4(\xi) \\ N_5(\xi) \end{Bmatrix} = \begin{bmatrix} 0.5 & 0 & 0 \\ 0.5 & 1 & 0.5 \\ 0 & 0 & 0.5 \end{bmatrix} \begin{Bmatrix} B_{1,2}\Big(\tilde{\xi}(\xi)\Big) \\ B_{2,2}\Big(\tilde{\xi}(\xi)\Big) \\ B_{3,2}\Big(\tilde{\xi}(\xi)\Big) \end{Bmatrix}, \quad \xi \in \Big[\frac{2}{12}, \frac{3}{12}\Big]. \tag{22}$$

From Equation (22) it is observed that the shape functions can be expressed as a linear combination of the Bernstein polynomials:

$$N_4(\xi) = 0.5B_{1,2}\Big(\tilde{\xi}(\xi)\Big) + B_{2,2}\Big(\tilde{\xi}(\xi)\Big) + 0.5B_{3,2}\Big(\tilde{\xi}(\xi)\Big). \tag{23}$$

Prepared using nmeauth.cls
DOI: 10.1002/nme

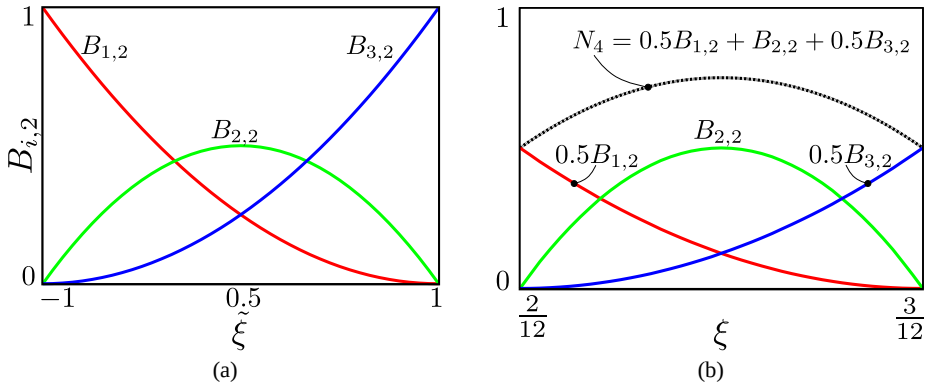

Figure 6. a) Quadratic Bernstein polynomials in the parent domain $\tilde{\xi} \in [-1, 1]$ - (b) Shape function N_4, in element 4 (parametric domain $\xi \in [2/12, 3/12]$), expressed as a linear combination of the Bernstein polynomials.

3.2. Isogeometric analysis with interfaces in two and three dimensions

To create meshes in higher-dimensional spaces, parametrisations in the y and the z-directions are introduced using the knot vectors $\mathcal{H} = [\eta_1, \eta_2, \cdots, \eta_{m+q+1}]$ and $\mathcal{Z} = [\zeta_1, \zeta_2, \cdots, \zeta_{o+r+1}]$, respectively. These knot vectors are associated with m basis functions of the order q, which are contained in $M_{j,q} (j \in \{1, m\})$, and o basis functions of the order r, contained in $O_{k,r} (k \in \{1, o\})$, respectively. The bivariate B-splines then follow from the tensor product of two knot vectors, resulting in a parametrisation $(\xi, \eta) \in \Xi \otimes \mathcal{H}$:

$$\mathbf{S}(\xi, \eta) = \sum_{i=1}^{n} \sum_{j=1}^{m} N_{i,p}(\xi) M_{j,q}(\eta) \mathbf{P}_{i,j}. \tag{24}$$

Similarly, the trivariate B-spline results from the parametrisation $(\xi, \eta, \zeta) \in \Xi \otimes \mathcal{H} \otimes \mathcal{Z}$:

$$\mathbf{S}(\xi, \eta, \zeta) = \sum_{i=1}^{n} \sum_{j=1}^{m} \sum_{k=1}^{o} N_{i,p}(\xi) M_{j,q}(\eta) O_{k,r}(\zeta) \mathbf{P}_{i,j,k}. \tag{25}$$

As for the univariate case, a Bézier operator can be defined in two and three dimensions as the tensor product of the univariate operators.

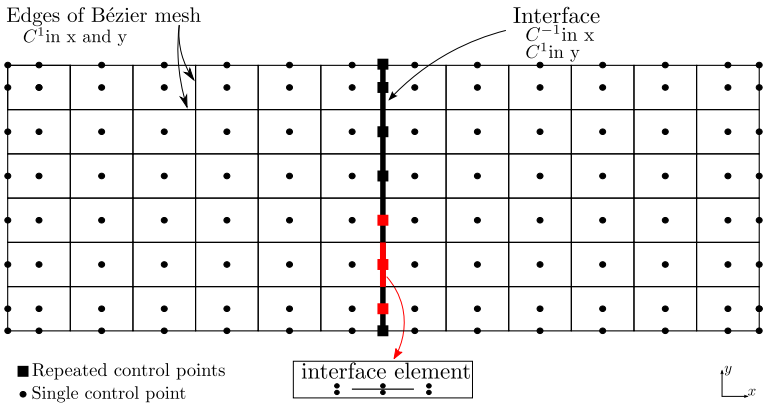

Figure 7. Quadratic two-dimensional mesh with a $\mathcal{C}^1$-interface depicted in the physical space. The knot vectors are: $\Xi = [0, 0, 0, \frac{1}{12}, \frac{2}{12}, \cdots, \frac{1}{2}, \frac{1}{2}, \frac{1}{2}, \cdots, 1, 1, 1]$ and $\mathcal{H} = [0, 0, 0, \frac{1}{6}, \frac{2}{6}, \frac{3}{6}, \frac{4}{6}, \frac{5}{6}, 1, 1, 1]$

As an example we consider a 12×6 quadratic two-dimensional mesh, Figure 7, which can be used to model the notched beam introduced in Figure 3a. The knot vector Ξ in the x-direction is the

DOI: 10.1002/nme

same as that used in Figure 5, i.e. with a discontinuity at $\xi = 0.5$. In the y-direction, the knot vector $\mathcal{H} = [0, 0, 0, \frac{1}{6}, \frac{2}{6}, \frac{3}{6}, \frac{4}{6}, \frac{5}{6}, 1, 1, 1]$ is used in order to obtain $\mathcal{C}^1$-continuity both in the bulk and along the interface. Figure 5 also shows that at the discontinuity, only one shape function is non-zero on either side in the ξ-direction: $N_8(\xi = 0.5^-) = N_9(\xi = 0.5^+) = 1$ in elements 6 and 7. This implies that the discontinuity can be described on each side as the univariate B-spline:

$$\mathbf{S}(\xi = 0.5, \eta) = \sum_{j=1}^{m} M_{j,q}(\eta)\mathbf{P}_{i,j}, \qquad i \in [1, n]. \tag{26}$$

Consequently, the $\mathbf{M}$-operator has the same structure as that for standard finite elements defined in Equation (15). The shape function along the interface becomes the univariate B-spline functions $M_{j,q}$ for the two-dimensional case, and for the three-dimensional case the bivariate B-spline functions $M_{j,q}O_{k,r}$ serve this purpose. Accordingly, the derivation of the internal and external force vectors and of the stiffness matrix, cf. Equations (16) and (17) also remains the same.

4. TRACTION OSCILLATIONS IN ISOGEOMETRIC INTERFACE ELEMENTS

4.1. Results with higher continuity along the interface

We revisit the notched beam of Figure 3a to assess the behaviour of the isogeometric interface elements, and consider $\mathcal{C}^1$-continuous quadratic and $\mathcal{C}^2$-continuous cubic isogeometric interface elements. Figure 8 shows the results for a two-dimensional analysis (and hence, one-dimensional interface elements). Quadratic B-splines with a three-point integration and cubic B-splines with a four-point integration scheme have been used for the interface elements. Results are shown both for Gauss quadrature and for Newton-Cotes integration. Compared to the standard finite element analysis, cf. Figure 3b, the results of the isogeometric analyses tend to aggravate the traction oscillations, especially near the tip of the notch, which is probably caused by the increased continuity. More importantly, and in contrast to standard interface elements, use of Newton-Cotes integration does not improve this unphysical behaviour, cf. [16]. Figure 9 shows that very similar results are obtained in three dimensions.

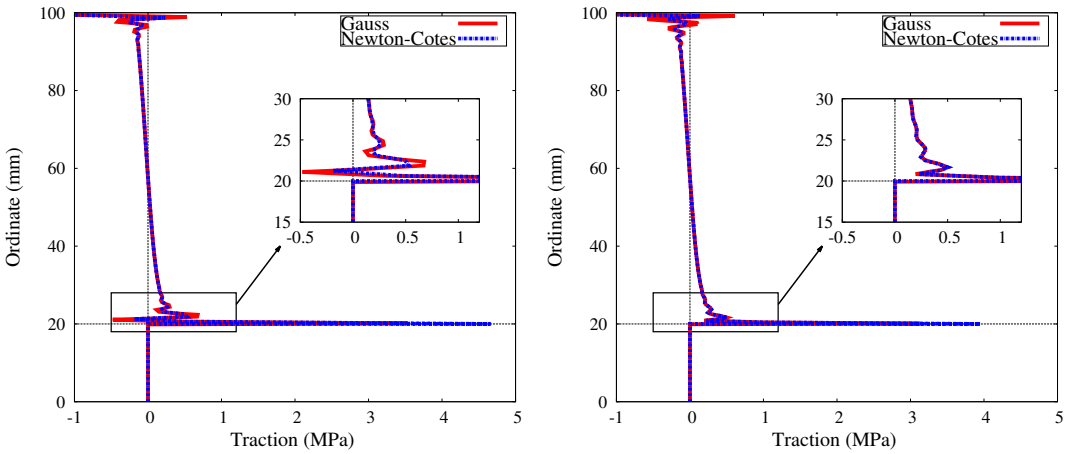

(a) quadratic B-spline (b) cubic B-spline

Figure 8. Results for two-dimensional analysis of the notched beam. Traction profile for (a) $\mathcal{C}^1$ and (b) $\mathcal{C}^2$-continuous interface elements using Gauss and Newton-Cotes integration with $k_n = 10^5 \text{N/mm}^3$. Three-point integration was used for the quadratic spline interpolation and a four-point rule was used for the cubic spline interpolation.

DOI: 10.1002/nme

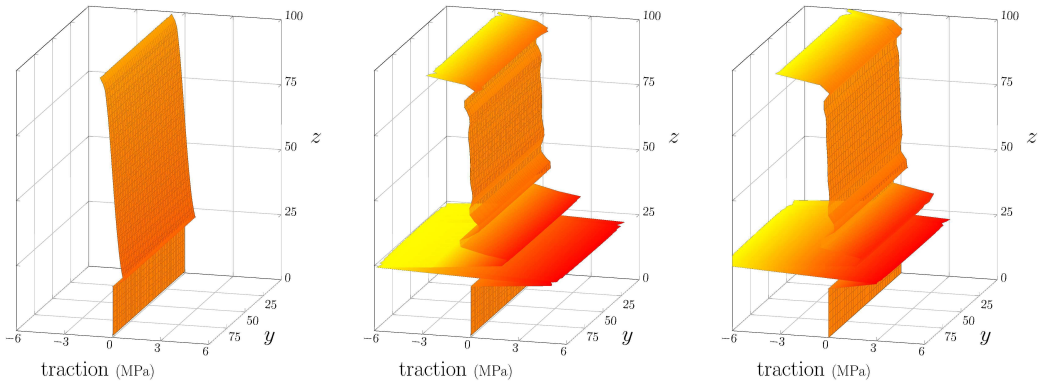

(a) Gauss integration k_n=10^{2}MPa/mm (b) Gauss integration k_n=10^{5}MPa/mm (c) Newton-Cotes integration k_n=10^{5}MPa/mm

Figure 9. Traction profiles along the interface for $\mathcal{C}^1$-continuous interface elements using Gauss and Newton-Cotes integration in three dimensions

4.2. Results for a $\mathcal{C}^0$-continuous interface

A key advantage of isogeometric analysis over standard finite element analysis is that the degree of continuity across element boundaries is easy to control using knot insertion [15]. This feature allows lowering the degree of continuity across element boundaries to $\mathcal{C}^0$ in the y-direction. By changing the knot vector $\mathcal{H}$ defined before into $\mathcal{H} = [0,0,0,\frac{1}{6},\frac{1}{6},\frac{2}{6},\frac{2}{6},\frac{3}{6},\frac{3}{6},\frac{4}{6},\frac{4}{6},\frac{5}{6},\frac{5}{6},1,1,1]$ (see the mesh in Figure 10), a discretisation is obtained that is $\mathcal{C}^0$-continuous at the element boundaries – like standard finite elements – but uses B-splines for the interpolation instead of the Lagrange polynomials used in standard finite elements.

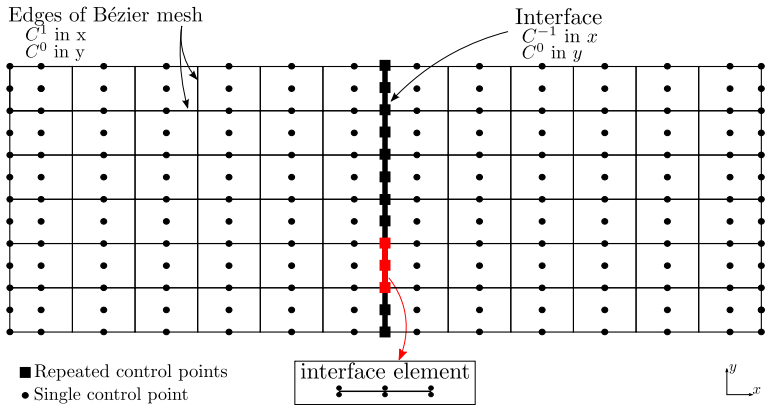

Figure 10. Quadratic mesh with $\mathcal{C}^0$-continuous interface elements. The knot vectors are: $\Xi = [0,0,0,\frac{1}{12},\frac{2}{12},\cdots,\frac{1}{2},\frac{1}{2},\frac{1}{2},\cdots,1,1,1]$ and $\mathcal{H} = [0,0,0,\frac{1}{6},\frac{1}{6},\frac{2}{6},\frac{2}{6},\frac{3}{6},\frac{3}{6},\frac{4}{6},\frac{4}{6},\frac{5}{6},\frac{5}{6},1,1,1]$

Figures 11 and 12 show that a reduction of the continuity to $\mathcal{C}^0$ along the interface makes the results of the isogeometric analysis resemble those of the standard finite element model. This observation holds for quadratic and for cubic shape functions, as well as for two-dimensional and three-dimensional analyses. As expected, Gauss integration still gives rise to traction oscillations along the interface, but, interestingly, the amplitude of these oscillations is lower, and is in the same order of magnitude as that when using Lagrange polynomials, cf. Figure 3b. The most striking observation is that the traction oscillations disappear when Newton-Cotes integration is used, similar to standard finite elements. Hence, the higher-order interelement continuity of isogeometric analysis

DOI: 10.1002/nme

seems to play an unfavourable role regarding the emergence of traction oscillations along the interface.

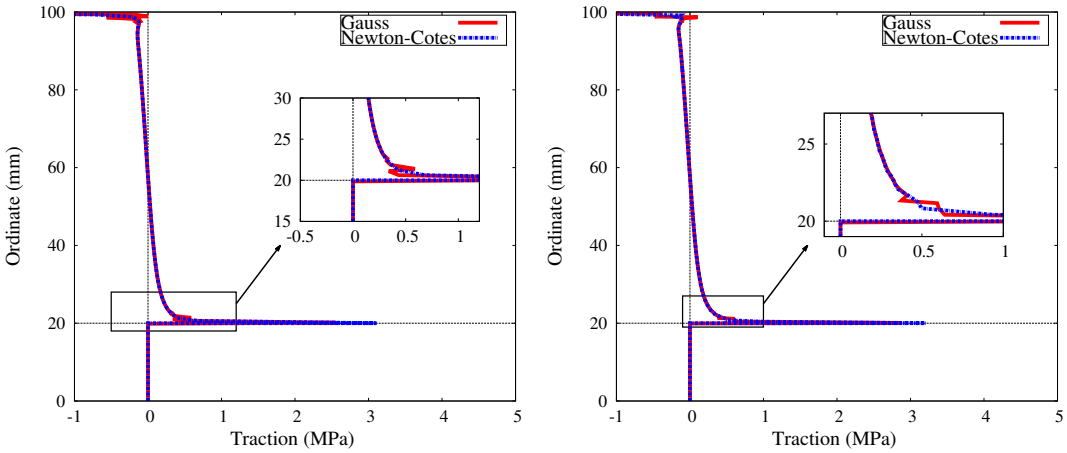

(a) quadratic B-spline (b) cubic B-spline

Figure 11. Traction profiles along the interface for $\mathcal{C}^0$-continuous interface elements using Gauss and Newton-Cotes integration schemes. Results in two dimensions for (a) quadratic, and (b) cubic B-splines with $k_n = 10^5$N/mm^3.

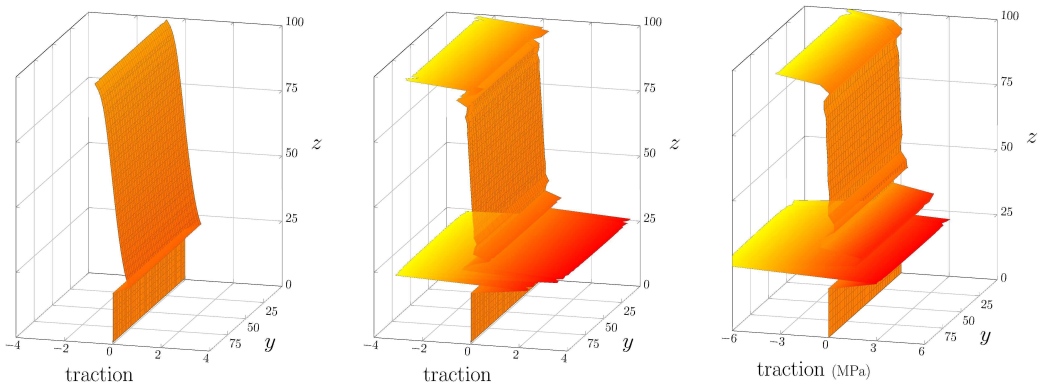

(a) Gauss integration k_n=10^{2}MPa/mm (b) Gauss integration k_n=10^{5}MPa/mm (c) Newton-Cotes integration k_n=10^{5}MPa/mm

Figure 12. Traction profiles along the interface for $\mathcal{C}^0$-continuous spline-based interface elements using Gauss and Newton-Cotes integration schemes in three dimensions

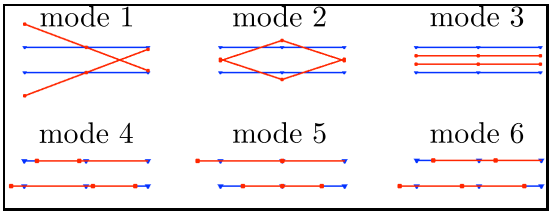

Figure 13. Eigenmodes of quadratic $\mathcal{C}^0$-continuous interface elements with a B-spline interpolation and using Newton-Cotes integration.

Prepared using nmeauth.cls
DOI: 10.1002/nme

The traction profiles of Figures 11 and 12 indicate that interface elements formulated within an isogeometric analysis framework and standard interface elements behave in a similar manner as when the interelement continuity is of the same order. However, there is a noteworthy difference as for the isogeometric interface elements, Newton-Cotes integration now does not result in node-set decoupling, yet results in smooth traction profiles. The coupling of the node-sets is clearly observed from the structure of the stiffness matrix:

$$\mathbf{K}^{\text{IGA-}\mathcal{C}^0}_{\text{Newton-Cotes}} = \frac{l}{12}\begin{bmatrix} 5k_n & -5k_n & 2k_n & -2k_n & k_n & -k_n \\ -5k_n & 5k_n & -2k_n & 2k_n & -k_n & k_n \\ 2k_n & -2k_n & 4k_n & -4k_n & 2k_n & -2k_n \\ -2k_n & 2k_n & -4k_n & 4k_n & -2k_n & 2k_n \\ k_n & -k_n & 2k_n & -2k_n & 5k_n & -5k_n \\ -k_n & k_n & -2k_n & 2k_n & -5k_n & 5k_n \end{bmatrix}, \tag{27}$$

which closely resembles that of Equation (18). As in Equation (18) only the stiffness terms that correspond to the u degrees of freedom have been printed for ease of readability. It also shows up in Figure 13, where the eigenmodes of $\mathbf{K}^{\text{IGA-}\mathcal{C}^0}_{\text{Newton-Cotes}}$ have been plotted in the physical space, so that points depict the displacements at the vertices and at the mid-points rather than at the control points. Similar as for the stiffness matrix that arises when using Gauss integration in conjunction with standard interface elements, $\mathbf{K}^{\text{FEM}}_{\text{Gauss}}$, the eigenmodes are coupled, cf. Figure 4a and Equation (18). Nonetheless, no traction oscillations are observed. This is an important result as it demonstrates that the oscillatory behaviour of the traction along the interface is not related to the node-set coupling [1]. It indicates that node-set decoupling is a sufficient rather than a necessary condition for removing oscillations in traction profiles for interface elements, either formulated using Lagrange polynomials, or using B-splines or NURBS.

Figure 14 reviews the relative locations of the integration points and the nodes/control points in the physical space for the cases considered in this study. It appears that for the two situations without traction oscillations, i.e. when using Newton-Cotes integration in conjunction with standard interface elements (FEM) and for the $\mathcal{C}^0$-continuous interface elements with a B-spline interpolation (IGA-$\mathcal{C}^0$), the integration points coincide with the nodes/control points (second row, first and third column, respectively). This coincidence could be a requirement for traction oscillations not to emerge, and the flexibility of isogeometric analysis allows to test this hypothesis. For this purpose the mid-control point is shifted in the model with $\mathcal{C}^0$-interelement continuity. This results in a shift of the mid-integration points as well, but by a different amount. This is because when the mid-control point is shifted, the Greville abscissae is no longer used. As a consequence, the Jacobian of the interface elements is no longer constant and the location of the centre of the element changes in the physical space. Consequently, the mid-control points and the mid-integration points no longer coincide. This is shown in the last row of Figure 14. The results for this case with Newton-Cotes integration do not exhibit traction oscillations, thus falsifying the hypothesis that the coinciding of integration points and nodes/control points is a necessary condition for traction oscillations not to appear.

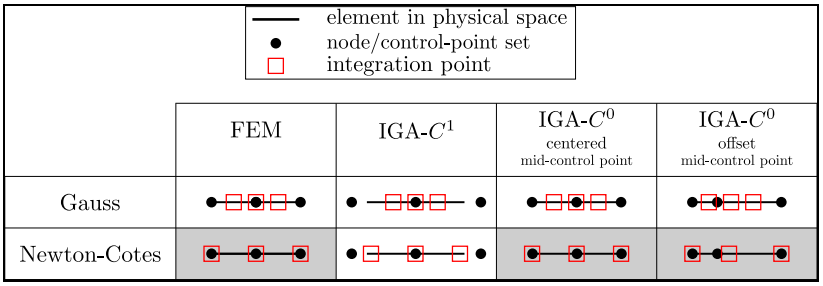

Figure 14. Relative location of integration points and nodes/control points. The cases without traction oscillations are shaded

DOI: 10.1002/nme

The literature invariably shows only traction oscillations, but not relative displacements, and notes that, when integrating interface elements with Gauss quadrature, the oscillations ameliorate when the dummy stiffness k_n is reduced. Figure 15 shows results for the relative displacement, or displacement jump, at the interface, using quadratic isogeometric interface elements, for Gauss integration as well as for Newton-Cotes integration. It is observed that, although the amplitude of the traction oscillations decreases for lower values of the dummy stiffness k_n, the oscillations in the jump field do not decrease, on the contrary. This observation holds irrespective of the integration scheme. The observation that oscillatory behaviour in the relative displacements also occurs for low values of the dummy stiffness is novel, and has been masked so far because in the plots of the traction oscillations they have been multiplied by the stiffness, and a lower stiffness then damps the oscillations in the tractions. The implication is that that the oscillatory nature is not driven by the magnitude of the dummy stiffness, but seems to be an inherent characteristic of interface elements.

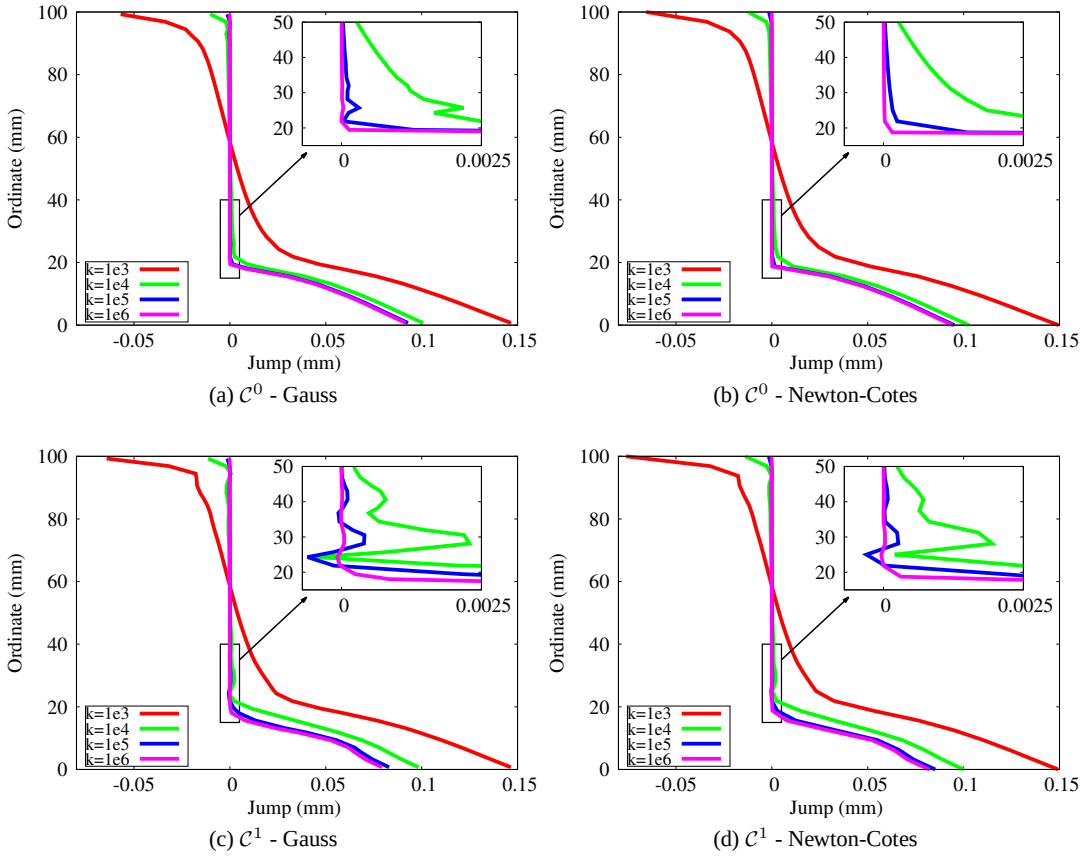

(a) $\mathcal{C}^0$ - Gauss (b) $\mathcal{C}^0$ - Newton-Cotes

(c) $\mathcal{C}^1$ - Gauss (d) $\mathcal{C}^1$ - Newton-Cotes

Figure 15. Jump profile along the interface for $\mathcal{C}^0$-continuous B-spline interfaces (a-b), and for $\mathcal{C}^1$-continuous B-spline interfaces (c-d)

It is finally noted that the condition number of the global stiffness matrix $\mathbf{K}$, see Equation (17), defined as the quotient of the largest and the smallest eigenvalue, does not appear to be of relevance regarding the occurrence of traction oscillations. This is observed from Figure 16, which gives the condition number as a function of the dummy stiffness, k_n, for standard interface elements and isogeometric interface elements with $\mathcal{C}^1$-interelement continuity, and different integration schemes. Moreover, tests with direct solvers as well as iterative solvers like conjugate gradients did not reveal any differences in the results.

DOI: 10.1002/nme

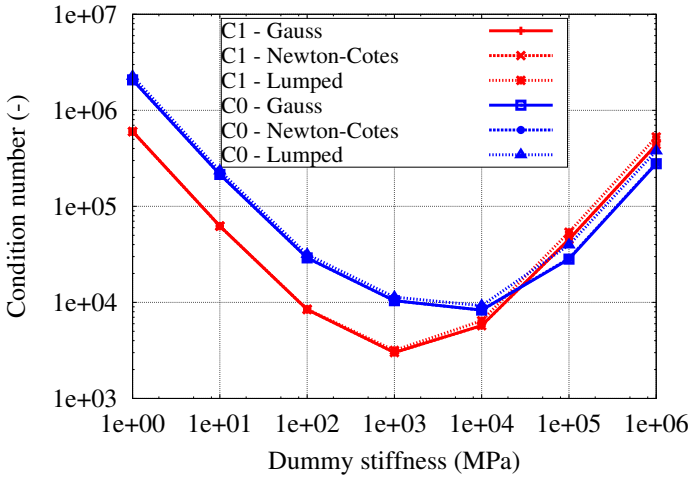

Figure 16. Condition number of the global stiffness matrix as a function of the dummy stiffness k_n. Results are also shown for lumped integration, which is discussed in Section 4.3.

4.3. Lumped integration

In [1] lumped integration has been investigated as an alternative integration scheme. The fundamental difference between lumped integration on one hand, and quadrature rules as Gauss or Newton-Cotes on the other hand, lies in the evaluation of the integral along the discontinuity that appears in the weak form, Equation (10). In Section 2 the discretisation was introduced into the weak form of Equation (11), together with interpolations of Equations (12) and (13), in order to obtain the internal force vector and the stiffness matrix of the interface elements. In the lumped integration scheme, rather than performing integration over elements, these integrals are evaluated in a discrete sense for each discrete set of control-points Scp, Figure 17.

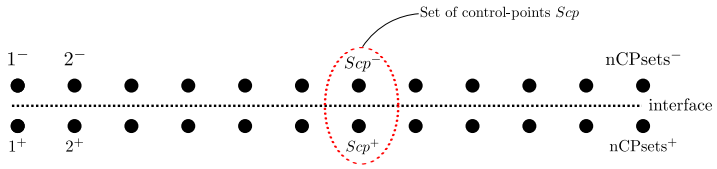

Figure 17. In the lumped integration scheme, interface elements are replaced by discrete sets of control points. For visualisation purposes the control points are shifted, but in reality coincide.

The element displacement vector at the interface, $\mathbf{u}_i^e$, is replaced by a vector which contains the displacements at a given set of control points Scp: $\mathbf{u}_{Scp}^e = \{u^-, u^+, v^-, v^+\}_{Scp}$. Hence, the displacement jump becomes a discrete quantity evaluated at each set of control points Scp, thus redefining the $\mathbf{M}_l$ operator, which now operates on single node-sets:

$$[\![\mathbf{u}]\!]_{Scp} = \begin{bmatrix} -1 & 1 & 0 & 0 \\ 0 & 0 & -1 & 1 \end{bmatrix} \begin{Bmatrix} u^- \\ u^+ \\ v^- \\ v^+ \end{Bmatrix}_{Scp} = \mathbf{M}_l \mathbf{u}_{Scp}. \tag{28}$$

The internal force vector then reads:

$$\mathbf{f}_{\text{interface}}^{\text{int}} = \sum_{Scp=1}^{\text{nCPsets}} \mathbf{M}_l^{\mathrm{T}} \mathbf{D}_i \mathbf{M}_l \mathbf{u}_{Scp}^e \tilde{A}_{Scp}, \tag{29}$$

where 'nCPsets' stands for the number of sets of control points and $\tilde{A}_{Scp}$ is a weighting factor accounting for the geometry of the interface attached to the node-set Scp (i.e.

DOI: 10.1002/nme

$\sum_{Scp=1}^{\text{nCPsets}} \tilde{A}_{Scp} = A_{\text{interface}}$). It is defined as:

$$\tilde{A}_{Scp} = \int_{\Gamma_d} N^{\pm}_{Scp} \, d\Gamma_d. \tag{30}$$

In Equation (30) $N^{\pm}_{Scp}$ denotes the shape function of either control point from the set Scp (on the $-$ side or on the $+$ side). This integral is evaluated using Gaussian integration in order to obtain the exact surface contribution. In essence, the lumped integration scheme replaces interface *elements* by *point-sets* at the interface, which can be interpreted as discrete springs.

It is observed from Figure 18 (two-dimensional configuration) and Figure 19 (three-dimensional configuration) that the traction oscillations disappear when using the lumped integration scheme. This holds for *all* cases considered, isogeometric interface elements with quadratic and cubic basis functions and $\mathcal{C}^0$-interelement continuity, quadratic basis functions with $\mathcal{C}^1$-interelement continuity, and cubic basis functions with $\mathcal{C}^2$-interelement continuity. It is noted that the magnitude of the traction singularity at the notch decreases for the lumped scheme.

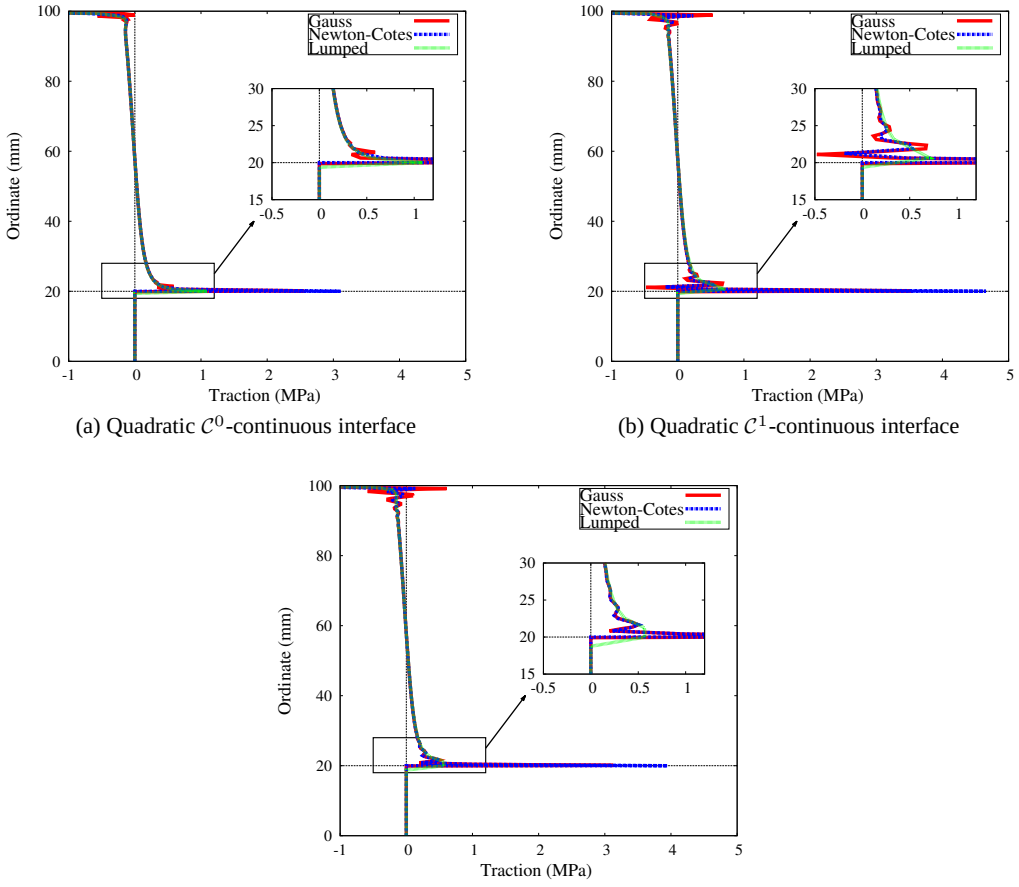

(a) Quadratic $\mathcal{C}^0$-continuous interface

(b) Quadratic $\mathcal{C}^1$-continuous interface

(c) Cubic $\mathcal{C}^2$-continuous interface

Figure 18. Traction profiles along the interface for $\mathcal{C}^0$, $\mathcal{C}^1$ and $\mathcal{C}^2$-continuous interface elements, using Gauss, Newton-Cotes and lumped integration schemes in two dimensions with $k_n = 10^5 \text{N/mm}^3$.

DOI: 10.1002/nme

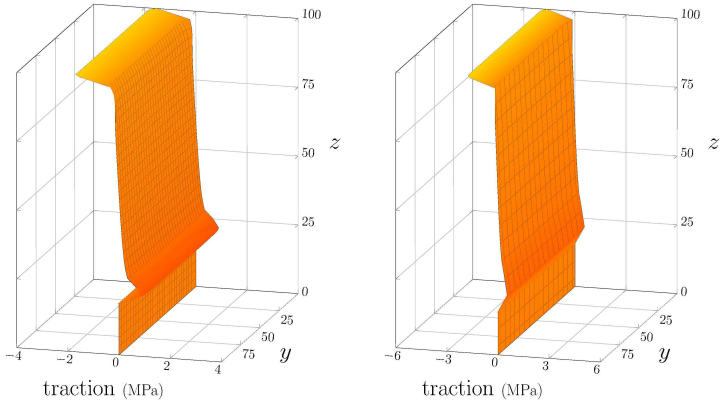

(a) $\mathcal{C}^0$-continuous interface (b) $\mathcal{C}^1$-continuous interface

Figure 19. Traction profile along the interface for (a) $\mathcal{C}^0$- and (b) $\mathcal{C}^1$-continuous interface using lumped integration in three dimensions for k_n=10^5MPa/mm

5. CONCLUSIONS

The numerical integration of isogeometric interface elements with a zero initial compliance has been investigated. In standard finite element analysis such elements are widely used to simulate cracking when the crack path is known in advance, e.g. in lamellar solids, or from experimental evidence. It turns out that, in line with an earlier, preliminary investigation [16], isogeometric interface elements share the oscillations in the tractions along interfaces also observed for standard interface elements. In fact, the higher continuity of isogeometric interface elements seems to aggravate the oscillations, and it is disturbing that a solution commonly adopted for standard interface elements, namely to adopt Newton-Cotes quadrature instead of Gauss quadrature, does not work for isogeometric finite elements. This paper demonstrates that the use of lumped integration is the only solution in the latter case, as this scheme has shown to be robust for two-dimensional and three-dimensional configurations, and for quadratic and cubic B-spline interpolations.

The investigations have revealed a number of interesting aspects about interface elements in general. First, node-set decoupling is not a necessary condition to remove traction oscillations along the interface, but rather seems to be a sufficient condition. Next, it has been shown by inspection of the relative displacements rather than the traction profiles at the interface, that the oscillatory response is not simply driven by high values of the dummy stiffness as it has been assumed so far, but seems to be inherent in the formulation of interface elements, either formulated in a standard manner, or within the framework of isogeometric analysis.

REFERENCES

1. Schellekens JCJ, de Borst R. On the numerical integration of interface elements, *International Journal for Numerical Methods in Engineering* 1993; **36**: 43–66.
2. de Borst R, Crisfield MA, Remmers JJC, Verhoosel CV (2012). *Non-Linear Finite Element Analysis of Solids and Structures*, 2nd Edition. John Wiley & Sons, Chichester, 2012.
3. Rots JG. Smeared and discrete representations of localized fracture, *International Journal of Fracture* 1991; **51**: 45–59.
4. Allix O, Ladevèze P. Interlaminar interface modelling for the prediction of delamination, *Composite Structures* 1992; **22**: 235–242.
5. Schellekens JCJ, de Borst R. A nonlinear finite-element approach for the analysis of mode 1 free edge delamination in composites, *International Journal of Solids and Structures* 1993; **30**: 1239–1253.
6. Schellekens JCJ, de Borst R. Free edge delamination in carbon-epoxy laminates: a novel numerical/experimental approach, *Composite Structures* 1994; **28**: 357–373.

DOI: 10.1002/nme

7. Alfano G, Crisfield MA. Finite element interface models for the delamination analysis of laminated composites: mechanical and computational issues, *International Journal for Numerical Methods in Engineering* 2001; **50**: 1701–1736.
8. Templeton EL, Rice JR. Off-fault plasticity and earthquake rupture dynamics: 1. Dry materials or neglect of fluid pressure changes, *Journal of Geophysical Research* 2008; **113**: B09306.
9. Xu XP, Needleman A. Numerical simulations of fast crack growth in brittle solids, *Journal of the Mechanics and Physics of Solids* 1994; **42**: 1397–1434.
10. Camacho GT, Ortiz M. Computational modelling of impact damage in brittle materials, *International Journal of Solids and Structures* 1996; **33**: 2899–2938.
11. Mergheim J, Kuhl E, Steinmann P. A hybrid discontinuous Galerin/interface method for the computational modelling of failure, *Communications in Numerical Methods in Engineering* 2004; **20**, 511–519.
12. Radovitsky R, Seagraves A, Tupek M, Noels L. A scalable 3D fracture and fragmentation algorithm based on a hybrid, discontinuous Galerkin cohesive method, *Computer Methods in Applied Mechanics and Engineering* 2011; **200**, 326–344.
13. de Borst R. Modern domain-based discretization methods for damage and fracture, *International Journal of Fracture* 2006; **138**, 241–262.
14. Verhoosel CV, Scott MA, de Borst R and Hughes TJR. An isogeometric approach to cohesive zone modeling, *International Journal for Numerical Methods in Engineering* 2011; **87**, 336-360.
15. Cottrell J, Hughes TJR, Bazilevs Y. *Isogeometric Analysis: Toward Integration of CAD and FEA.* John Wiley & Sons, Chichester, 2009.
16. Irzal, F, Remmers JJC, Verhoosel CV, de Borst R. An isogeometric analysis Bézier interface element for mechanical and poromechanical fracture problems, *International Journal for Numerical Methods in Engineering* 2014; **87**, 608–628.
17. Nguyen VP, Nguyen-Xuan H. High order B-splines based finite elements for the delamination analysis of laminated composites, *Composite Structures* 2013; **102**, 261–275.
18. Nguyen VP, Kerfriden P, Bordas S. Two- and three-dimensional isogeometric cohesive elements for composite delamination analysis, *Composites Part B* 2014; **60**, 193–212.
19. Borden MJ, Scott MA, Evans JA, Hughes TJR. Isogeometric finite element data structures based on Bézier extraction of NURBS. *International Journal for Numerical Methods in Engineering* 2011; **87**: 15–47.
20. Scott MA, Borden MJ, Verhoosel CV, Sederberg TW, Hughes TJR. Isogeometric finite element data structures based on Bézier extraction of T-splines. *International Journal for Numerical Methods in Engineering* 2011; **88**: 126–156.
21. Greville T. Numerical procedures for interpolation by spline functions, *SIAM Journal of Numerical Analysis* 1964; **1**: 53–68.
22. Cox MG. The numerical evaluation of B-splines. *IMA Journal of Applied Mathematics* 1972; **10**: 134-149.
23. de Boor C. On calculating with B-splines. *Journal of Approximation Theory* 1972; **6**: 50-62.

DOI: 10.1002/nme